Editors' Suggestion

Polarization-controlled supercurrent in ferroelectric Josephson junctions

Yaozu Tang [1,2] Mazhar N. Ali [1,2] Gerrit E. W. Bauer [3,4] and Yaroslav M. Blanter [1,2]

[1] *Kavli Institute of Nanoscience, Delft University of Technology, Lorentzweg 1, 2628 CJ Delft, The Netherlands*

[2] *Department of Quantum Nanoscience, Delft University of Technology, Lorentzweg 1, 2628 CJ Delft, The Netherlands*

[3] *WPI-AIMR & IMR & CSIS, Tohoku University, 2-1-1 Katahira, Sendai 980-8577, Japan*

[4] *Kavli Institute for Theoretical Sciences, University of the Chinese Academy of Sciences, Beijing 10090, China*

(Received 19 November 2025; accepted 3 March 2026; published 10 April 2026)

Josephson junctions are essential devices in superconducting electronics and quantum computing hardware. Here we predict electrical control of the supercurrent in composite superconductor-insulator-ferroelectric-insulator-superconductor (S-I-FE-I-S) Josephson junctions. Inversion symmetry broken by unequal dielectric barrier thicknesses and/or potentials converts ferroelectric polarization reversal into a substantial change of the critical current. Using a WKB approximation, we model the nonvolatile switching of the critical current with on-off efficiency that is tunable by thicknesses and potential barriers of the insulating layers, as well as the thickness and dielectric constant of the ferroelectric layer. We also derive a compact linear expression for the critical current valid for small polarizations. Our results identify ferroelectric Josephson junctions as electrically programmable superconducting current switches for cryogenic memory and logic applications.

DOI: 10.1103/nvbk-27dx

I. INTRODUCTION

The Josephson effect, where a supercurrent flows through a junction formed by two superconductors separated by a weak link [1–3], is a cornerstone phenomenon in condensed matter physics. It underpins a wide range of applications, including superconducting qubits [4–8], SQUID sensors [9–11], and superconducting single-photon detectors [12–14]. The incorporation of diverse quantum materials (QMs), including semiconducting nanowires [15–18], ferromagnets [19–28], and topological materials [29–34], has further expanded the functionality of Josephson junctions (JJs). The three-terminal Josephson field effect transistor (JoFET) is a promising cryogenic logic device based on the electric control of the supercurrent [35–41].

Ferroelectric materials, characterized by their spontaneous and switchable electric dipolar order, have been widely utilized in applications ranging from memory devices to sensors [42–50]. However, their integration as weak links in Josephson junctions remains underexplored, and the interplay between ferroelectric polarization and superconductivity has not yet been fully understood. A notable feature of ferroelectric materials is the giant tunneling electroresistance (TER) observed in ferroelectric tunnel junctions (FTJs), in which a nanometer-thick ferroelectric layer acts as the tunneling barrier between metallic electrodes [51–54]. Due to the resistive switching upon polarization reversal and the gradual tunability of the resistance, FTJs have been considered as candidates for nonvolatile memory and neuromorphic computing architectures [55–59]. This implies that ferroelectric Josephson junctions could exhibit unique properties with potential applications in cryogenic memory and computation [60].

Recently, directional supercurrent rectification—the superconducting diode effect—has attracted considerable attention [61–65]. This effect typically relies on broken inversion and time-reversal symmetries, often via magnetic textures or fields [64–66]. However, for scalable and power-saving device applications, local electrical control is highly desirable. Here, we propose an all-electrical route to strongly modulate (switch) the critical current via electric polarization, which offers an alternative for controllable superconducting devices without invoking magnetism. The modulation of supercurrent by a nonvolatile ferroelectric polarization causes the memory [67] and diode effects [68] in ferroelectric Josephson junctions.

We analyze a composite S-I-FE-I-S junction in which a ferroelectric layer is sandwiched between two (para/dielectric) insulating layers with independently tunable thicknesses and potential barrier heights. The reversal of a perpendicular electrical polarization shifts the electrostatic potential profiles. With broken inversion symmetry of the stacking, the normal state conductance, and thus the critical current, differ for different polarization directions. We find a polarization-controlled on-off efficiency that can approach 0.9 for physically realistic parameters and identify trade offs with absolute current magnitude. We also derive a compact linear formula for the polarization dependence of the critical current valid at small polarization, offering rapid estimates for device modeling and design.

The manuscript is organized as follows: In Sec. II, we present our tunneling model of the composite ferroelectric Josephson junction. In Sec. III, we discuss the polarization dependence of the critical current as well as how the on-off efficiency can be tuned by adjusting the system parameters. In Sec. IV, we present analytical expressions of the critical

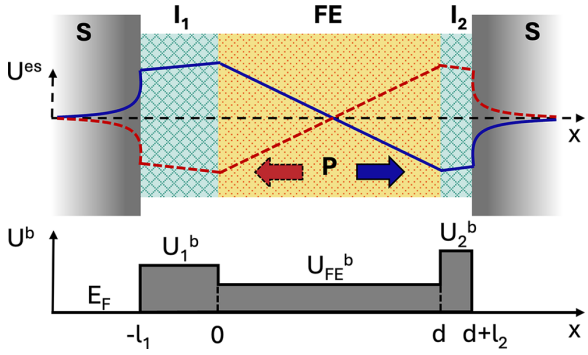

FIG. 1. S-I-FE-I-S composite ferroelectric junction. Top: Geometry and electrostatic potential U^{es} for opposite polarization directions (blue vs red). Bottom: An asymmetric potential barrier profile U^b in the dielectric state.

current in the limit of small polarization. Finally, in Sec. V, we summarize our findings and present an outlook.

II. S-I-FE-I-S MODEL

We consider a composite superconductor-insulator-ferroelectric-insulator-superconductor (S-I_1-FE-I_2-S) junction (Fig. 1) with broken inversion symmetry as a minimal model. The nonferroelectric electrically insulating layers, I_1 and I_2, form potential barriers with heights U_1^b and U_2^b and thicknesses l_1 and l_2. We assume here that the superconductors (S) on both sides are the same. The ferroelectric (FE) is an electrical insulator with thickness d that forms a potential barrier U_f^b in its dielectric state (see bottom panel of Fig. 1). Its polarization P is uniform and normal to the interfaces. The polarization induces equal and opposite bound charges at the FE interfaces, which are screened by free carriers in the metallic electrodes [51]. The resulting electrostatic potential U^{es} is linear inside the ferroelectric and decays exponentially in the metals over the (Thomas-Fermi) screening length. The total potential profile entering the tunneling problem is the sum

$$U(x) = U^{es}(x) + U^b(x).$$

We derive in the following that when inversion symmetry is broken, reversing P changes U^{es}, the electrical conductance, and the critical current.

The electrostatic potential in the metallic electrodes is described by the Thomas-Fermi screening model [51,69]:

$$U^{es}(x) = \begin{cases} \varepsilon_0^{-1}\sigma_s\delta\, e^{-|x+l_1|/\delta}, & x \leqslant -l_1, \\ -\varepsilon_0^{-1}\sigma_s\delta\, e^{-|x-(d+l_2)|/\delta}, & x \geqslant d+l_2, \end{cases} \tag{1}$$

where σ_s is the surface screening charge density and δ the screening length. For normal metals, δ is the Thomas-Fermi length $\delta_{TF}^2 = 2\varepsilon_0 E_F/3e^2 n$, and is typically below 1 nanometer for high-density metals. Here E_F is the Fermi energy and n the electron density. In superconductors, the appropriate screening length is being debated: Whether it remains the same as the normal-state Thomas-Fermi length or is given by the much larger London penetration depth [70–73]. In this paper we adopt $\delta = \delta_{TF}$ for the main calculations and comment on the consequences of larger δ at the end of Sec. III.

Inside the ferroelectric, the electric field

$$\frac{U^{es}(0) - U^{es}(d)}{d} = \frac{P - \sigma_s}{\varepsilon_f \varepsilon_0} \tag{2}$$

is constant and ε_f is the ferroelectric dielectric constant. $P > 0$ indicates polarization pointing toward I_2, and the electric fields in the insulating spacer layers follow:

$$\frac{U^{es}(0) - U^{es}(-l_1)}{l_1} = \frac{\sigma_s}{\varepsilon_1\varepsilon_0}, \qquad \frac{U^{es}(l_2+d) - U^{es}(d)}{l_2} = \frac{\sigma_s}{\varepsilon_2\varepsilon_0}, \tag{3}$$

with $\varepsilon_{1,2}$ the dielectric constants of $I_{1,2}$.

Solving Eqs. (1)–(3) yields

$$\sigma_s = \beta P, \tag{4}$$

$$U^{es}(0) = \frac{1}{\varepsilon_0}\left(\delta + \frac{l_1}{\varepsilon_1}\right)\beta P, \tag{5}$$

$$U^{es}(d) = \frac{1}{\varepsilon_0}\left(\delta + \frac{l_2}{\varepsilon_2}\right)\beta P, \tag{6}$$

with the form factor

$$\beta = \frac{d/\varepsilon_f}{d/\varepsilon_f + l_1/\varepsilon_1 + l_2/\varepsilon_2 + 2\delta}. \tag{7}$$

Reversing the polarization changes the sign of P, and thus of $U^{es}(x)$ (Fig. 1). For thin barriers with large dielectric constant such that $l_1/\varepsilon_1,\ l_2/\varepsilon_2 \ll \delta$, Eqs. (4)–(6) simplify to

$$\sigma_s = \frac{d/\varepsilon_f}{d/\varepsilon_f + 2\delta} P, \tag{8}$$

$$U^{es}(0) = -U^{es}(d) = \frac{d/\varepsilon_f}{d/\varepsilon_f + 2\delta}\frac{\delta}{\varepsilon_0} P \equiv \Delta_p. \tag{9}$$

In this limit U^{es} is constant across $I_{1,2}$. In the following, for simplicity we focus on this experimentally relevant regime.

III. POLARIZATION-CONTROLLED CRITICAL CURRENT AND TUNABLE ON-OFF EFFICIENCY

The supercurrent $I_s = I_c \sin\phi$ depends on the phase difference ϕ across the Josephson junction. At zero temperature, the critical current density $J_c = I_c/A$ of a short tunnel junction with area A reads [3,74]

$$J_c = \frac{\pi\Delta_0}{2e}\frac{G_N}{A}, \tag{10}$$

where Δ_0 is the superconducting gap and $G_N = (2e^2/h)\sum_n T_n$ is the normal-state conductance expressed as a sum over spin-degenerate transmission eigenvalues T_n. Equation (10) holds for junctions with a weak link shorter than the superconducting coherence length, which is the case for our nanometer-thin barriers.

The Landauer formula for the conductance reads in the free-electron approximation,

$$\frac{G_N}{A} = \frac{2e^2}{h}\int_0^{k_F} \frac{k_{||}\, dk_{||}}{2\pi}\, T(E, k_{||}), \tag{11}$$

where $k_{||} = \sqrt{k_y^2 + k_z^2}$, and k_F is the Fermi wave vector. Numerical calculations of the transmission $T(E, k_{||})$ through the

composite barrier for high density metals suffer from rapid oscillations that average out to a large extent in the integral. These oscillation are suppressed in the Wentzel-Kramers-Brillouin (WKB) approximation [75],

$$T(E,k_{||}) \approx \exp\left[-2\int_{-l_1}^{d+l_2}\frac{\sqrt{2m\left(E_F+U-\left(E-\frac{\hbar^2k_{||}^2}{2m}\right)\right)}}{\hbar}dx\right], \tag{12}$$

that holds for sufficiently large potential barriers for which the square root is real.

The total potential $U(x)$ depends on the electric polarization P, and so does J_c. Two figures of merit are the (dimensionless) on-off efficiency

$$\eta(P)=\frac{|J_c(+P)-J_c(-P)|}{J_c(+P)+J_c(-P)}\leqslant 1, \tag{13}$$

that measures the relative change of J_c upon polarization reversal, and the polarization-averaged critical current density,

$$\bar{J}_c(P)=\frac{J_c(+P)+J_c(-P)}{2}. \tag{14}$$

Unless stated otherwise, we use the following material parameters: superconducting gap $\Delta_0=2$ meV (reasonable for elemental s-wave superconductors such as Nb and Pb [76]); Fermi energy $E_F=5$ eV (Nb [77]); transmission energy at $E=E_F$; Thomas-Fermi screening length in high density metals $\delta=0.1$ nm [78]; ferroelectric thickness $d=2$ nm; and ferroelectric intrinsic barrier $U_f^b=0.1$ eV [79]. The ferroelectric dielectric constant is considered highly material and temperature dependent, thus we take a moderate value of $\varepsilon_f=100$ [80], representative for ferroelectric perovskites and comment on the consequences of smaller and larger values at the end of this section.

Figure 2 shows four representative geometries of the potential profiles. The corresponding $\bar{J}_c(P)$ and $\eta(P)$ are plotted in Fig. 3. In the symmetric junction [Fig. 2(a)], inversion symmetry guarantees $J_c(+P)=J_c(-P)$ and thus $\eta=0$. Introducing asymmetric potential barriers [Fig. 2(b)] lowers $\bar{J}_c$ and monotonically raises η with $|P|$. Different thicknesses but equal potential barriers [Fig. 2(c)] lead to the same conclusion. Combining thickness and barrier asymmetries [Fig. 2(d)] enhances the efficiency up to $\eta\approx 0.9$ for $P=8$ μC/cm^2, but at the cost of a small critical current density of a few nA/μm^2.

We assess the tunability for fixed $|P|=5$ μC/cm^2 and different structural parameters. Figures 4(a) and 4(b) show that the efficiency improves with both thickness and barrier asymmetry. Varying both simultaneously [Fig. 4(c)] can cancel the modulation efficiency for some parameter combinations: the line cuts in Fig. 4(d) emphasize that for $l_1\neq l_2$ the efficiency goes to zero. On the other hand, η is maximized when the thinner (thicker) insulating layer has a larger (smaller) potential barrier, respectively.

Figure 5(a) illustrates that the efficiency increases with ferroelectric thickness d and decreases with dielectric constant ε_f, consistent with an electrostatic potential change that scales like $\Delta_p\propto 1/(\varepsilon_f/d+\text{const.})$ [Eq. (9)]. Thicker ferroelectric layers enhance the internal potential drop and hence

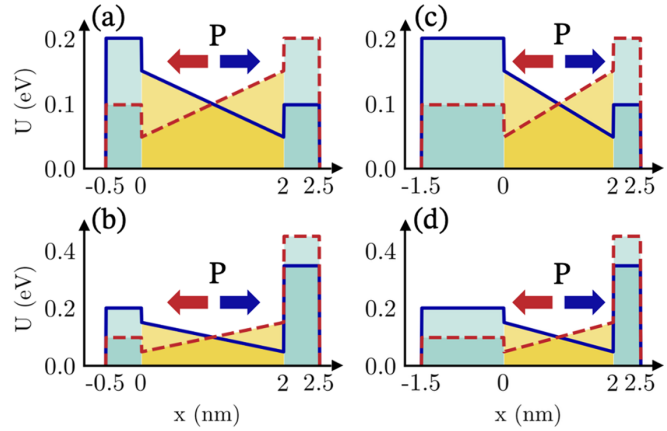

FIG. 2. Potential profiles. Ferroelectric (yellow) and dielectric (blue) layers. Blue (solid) and red (dashed) curves: total potentials for opposite polarization directions (arrows). (a) Symmetric junction: $l_1=l_2=0.5$ nm, $U_1^b=U_2^b=0.15$ eV. (b) Barrier asymmetric: $l_1=l_2=0.5$ nm, $U_1^b=0.15$ eV, $U_2^b=0.4$ eV. (c) Thickness asymmetric: $U_1^b=U_2^b=0.15$ eV, $l_1=1.5$ nm, $l_2=0.5$ nm. (d) Strongly asymmetric: $l_1=1.5$ nm, $l_2=0.5$ nm, $U_1^b=0.15$ eV, $U_2^b=0.4$ eV.

the contrast between $\pm P$, but large total barrier thickness also suppresses the modulus of the critical current. A smaller dielectric constant increases the efficiency, but also implies a smaller $|J_c|$. Figure 5(b) examines the role of the screening length δ. By rewriting Eq. (9) as

$$\Delta_p=\frac{1/\varepsilon_0}{2\varepsilon_f/d+1/\delta}P, \tag{15}$$

we see that for large ε_f, as in many ferroelectric perovskites, the ferroelectric contribution dominates the electrostatic potential and η is largely insensitive to δ. For materials with smaller ε_f (for example $CuInP_2S_6$ [81–83] or HfO_2 [50,84,85]), the ferroelectric control of the potential is weaker and η tends to benefit from a larger screening length [Eq. (9)], although this dependence is modest in realistic regimes ($\delta\gtrsim 0.1$ nm). A comprehensive optimization of η and J_c across realistic layer structures, susceptibilities, and material polarizations is beyond the scope of this work.

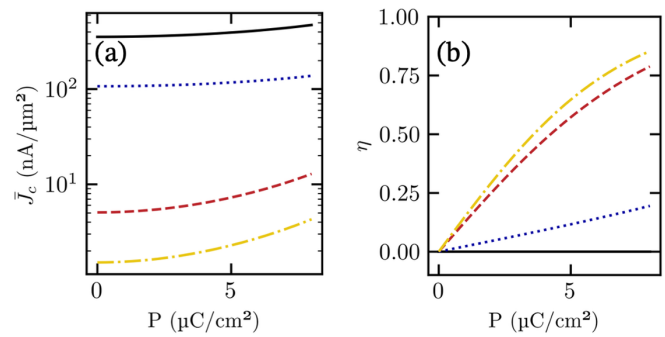

FIG. 3. Polarization dependence. (a) Averaged critical current density $\bar{J}_c$ and (b) on-off efficiency η vs polarization P. Solid black: symmetric junction of Fig. 2(a). Dotted blue: barrier asymmetry [Fig. 2(b)]. Dashed red: thickness asymmetry [Fig. 2(c)]. Dash-dot yellow: combined strong asymmetry [Fig. 2(d)].

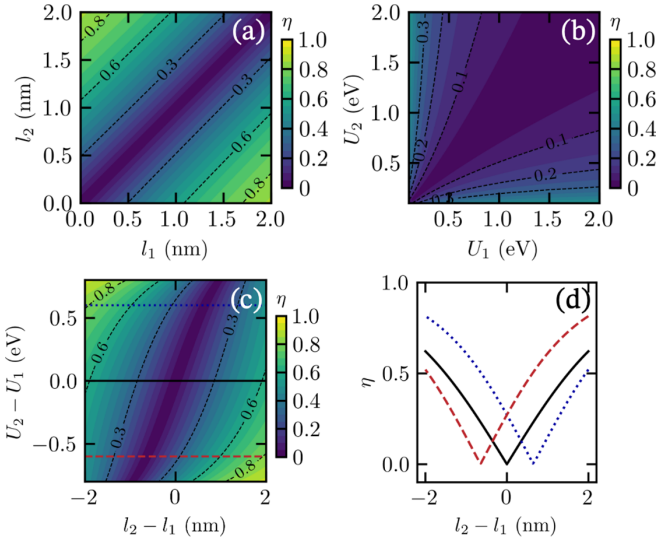

FIG. 4. Tunable on-off efficiency at fixed $|P| = 5\ \mu\text{C/cm}^2$. (a) η vs l_1, l_2 for $U_1^b = U_2^b = 0.15$ eV. (b) η vs U_1^b, U_2^b for $l_1 = l_2 = 1.0$ nm. (c) η vs thickness difference $l_2 - l_1$ and barrier difference $U_2^b - U_1^b$ at fixed $l_1 + l_2 = 2$ nm and $U_1^b + U_2^b = 1$ eV. (d) Line cuts of (c): η vs $l_2 - l_1$ for $U_2^b - U_1^b = 0$ (solid black), $+0.6$ eV (dotted blue), and -0.6 eV (dashed red).

IV. LINEAR APPROXIMATION OF CRITICAL CURRENT

Here we study a small-parameter expansion of the polarization-dependent critical current starting from Eqs. (11) and (12).

The integral in Eq. (12) can be separated into contributions from the three layers:

$$T(k_{||}) \approx e^{-2(\gamma_1+\gamma_2+\gamma_f)}, \tag{16}$$

where

$$\gamma_1 = l_1\sqrt{\frac{2mU_1}{\hbar^2} + k_{||}^2}, \tag{17}$$

$$\gamma_2 = l_2\sqrt{\frac{2mU_2}{\hbar^2} + k_{||}^2}, \tag{18}$$

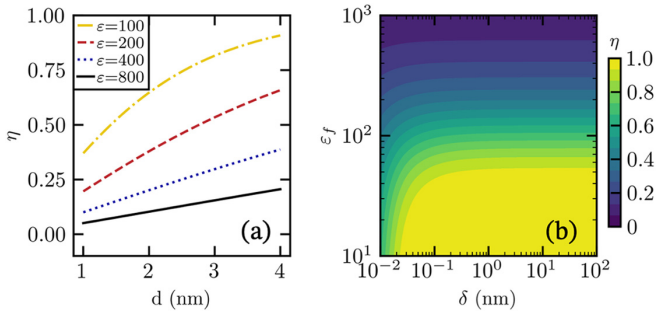

FIG. 5. Dependence on ferroelectric thickness, dielectric constant, and screening length. (a) η vs ferroelectric thickness d for a strongly asymmetric junction in Fig. 2(d) and dielectric constants $\varepsilon_f = 800$ (solid black), 400 (dotted blue), 200 (dashed red), and 100 (dash dot yellow). The screening length $\delta = 0.1$ nm. (b) η vs screening length δ and ε_f for $d = 2$ nm.

$$\gamma_f = \frac{2}{3}\frac{d\hbar^2}{2m[U_f(d) - U_f(0)]} \times \left\{\left[\frac{2mU_f(d)}{\hbar^2} + k_{||}^2\right]^{\frac{3}{2}} - \left[\frac{2mU_f(0)}{\hbar^2} + k_{||}^2\right]^{\frac{3}{2}}\right\}, \tag{19}$$

are the WKB exponents for the two insulating layers and the ferroelectric layer, respectively. $U_1 = U_1^b + \Delta_p$ and $U_2 = U_2^b - \Delta_p$ are the total potential barriers of the insulating layers, while $U_f(0) = U_f^b + \Delta_p$ and $U_f(d) = U_f^b - \Delta_p$ are those at their interfaces to the ferroelectric and Δ_p is the polarization-induced electrostatic offset in Eq. (9).

For sufficiently small $k_{||}$ or high barriers $k_{||}^2 \ll 2mU/\hbar^2$, we may expand the square roots to obtain

$$\gamma_1 \approx \frac{l_1\sqrt{2mU_1}}{\hbar} + \frac{1}{2}\frac{l_1\hbar}{\sqrt{2mU_1}}k_{||}^2, \tag{20}$$

$$\gamma_2 \approx \frac{l_2\sqrt{2mU_2}}{\hbar} + \frac{1}{2}\frac{l_2\hbar}{\sqrt{2mU_2}}k_{||}^2, \tag{21}$$

$$\gamma_f \approx \frac{2}{3}\frac{d\sqrt{2m}[U_f(0)^{3/2} - U_f(d)^{3/2}]}{\hbar[U_f(0) - U_f(d)]} + \frac{d\hbar[\sqrt{U_f(0)} - \sqrt{U_f(d)}]}{\sqrt{2m}[U_f(0) - U_f(d)]}k_{||}^2. \tag{22}$$

When additionally $\Delta_p/U^b \ll 1$, the transmission takes the form

$$T(k_{||}, \Delta_p) = e^{-(A_p + B_p k_{||}^2)}, \tag{23}$$

where A_p and B_p are polarization-dependent coefficients:

$$A_p = 2\frac{\sqrt{2m}}{\hbar}\left[l_1\sqrt{U_1^b} + l_2\sqrt{U_2^b} + d\sqrt{U_f^b} - \frac{1}{2}\left(\frac{l_2}{\sqrt{U_2^b}} - \frac{l_1}{\sqrt{U_1^b}}\right)\Delta_p\right], \tag{24}$$

$$B_p = \frac{\hbar}{\sqrt{2m}}\left\{\frac{l_1}{\sqrt{U_1^b}} + \frac{l_2}{\sqrt{U_2^b}} + \frac{d}{\sqrt{U_f^b}}\right. \tag{25}$$

$$\left. + \frac{1}{2}\left[\frac{l_2}{(U_2^b)^{\frac{3}{2}}} - \frac{l_1}{(U_1^b)^{\frac{3}{2}}}\right]\Delta_p\right\}. \tag{26}$$

In this limit the Landauer integral Eq. (11) can be evaluated analytically when k_F is much larger than the scale over which the Gaussian-like integrand $k_{||}e^{-(A_p+B_pk_{||}^2)}$ vanishes. We introduce a cutoff $k_c \equiv 1/\sqrt{B_p}$, for which the small $k_{||}$ approximation holds. The critical current density then simplifies to

$$J_c = \frac{e\Delta_0}{2h}\frac{e^{-A_p}}{2B_p}\left[1 - e^{-B_pk_c^2}\right] \approx \frac{e\Delta_0}{2h}\frac{e^{-A_p}}{2B_p}. \tag{27}$$

To first order in $\Delta_p \sim P$ we get

$$J_c(P) = \frac{e\Delta_0}{4h}\kappa(1 + \theta P), \tag{28}$$

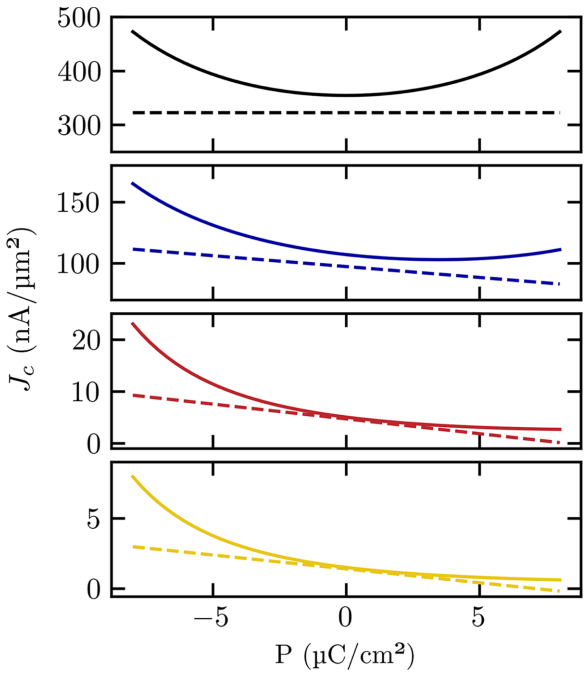

FIG. 6. Linear approximation of the polarization dependence of the critical current density. Critical current density J_c vs polarization P. (a)–(d) correspond to the junctions in Figs. 2(a)–2(d). Solid: numerical results; dashed: analytical approximation.

and

$$\eta(P) = |\theta P|, \tag{29}$$

where κ and θ are device-dependent coefficients:

$$\kappa = \frac{\exp\left\{-2\frac{\sqrt{2m}}{\hbar}\left(l_1\sqrt{U_1^b} + l_2\sqrt{U_2^b} + d\sqrt{U_f^b}\right)\right\}}{\frac{\hbar}{\sqrt{2m}}\left(l_1/\sqrt{U_1^b} + l_2/\sqrt{U_2^b} + d/\sqrt{U_f^b}\right)}, \tag{30}$$

$$\theta = \frac{d\delta/\epsilon_0}{d + 2\delta\epsilon_f}\left[\frac{l_1/\left(U_1^b\right)^{3/2} - l_2/\left(U_2^b\right)^{3/2}}{l_1/\sqrt{U_1^b} + l_2/\sqrt{U_2^b} + d/\sqrt{U_f^b}} - \frac{\sqrt{2m}}{\hbar}\left(\frac{l_1}{U_1^b} - \frac{l_2}{U_2^b}\right)\right]. \tag{31}$$

Figure 6 compares the numerical and analytical results of the critical current density. The linear approximation captures both magnitude and trend for small $|P|$. The slight offset at $P = 0$ arises from the small-$k_{||}$ assumption in the WKB integral and the approximation taken in the second step of Eq. (27). The compact formulas in Eqs. (28) and (29) thus provide rapid estimates of polarization control in ferroelectric Josephson junctions.

V. CONCLUSIONS

We analyzed the behavior of a composite S-I_1-FE-I_2-S Josephson junction. When breaking inversion symmetry by different thicknesses and/or heights of the potential barriers that separate the ferroelectric from the superconductor, a ferroelectric polarization reversal strongly modulates the critical current. In a WKB approximation we compute an electrically controlled on-off efficiency up to $\eta \simeq 0.9$ for physically realistic parameters. The efficiency η can be maximized by thicknesses and potential barrier heights that are larger and lower on one side than on the other, in thicker ferroelectric films with large polarization, but small dielectric constant. We derive a compact formula in the limit of small P for quick estimates and interpreting numerical results. We conclude that ferroelectric Josephson junctions are interesting candidates for electrically programmable superconducting current switches in cryogenic memories and logic circuits.

ACKNOWLEDGMENTS

The authors would also like to thank the Kavli Foundation for their support through the Kavli Institute Innovation Award and The Kavli Institute of Nanoscience Delft. M.N.A. acknowledges the support of the NWO Talent Programme VIDI financed by the NWO VI.Vidi.223.089. G.E.W.B. was supported by the Japan Society for the Promotion of Science, Kakenhi Grants No. 22H04965 and No. JP24H02231.

DATA AVAILABILITY

The data that support the findings of this article are openly available [86].

[1] B. D. Josephson, Possible new effects in superconductive tunnelling, Phys. Lett. **1**, 251 (1962).
[2] B. D. Josephson, Supercurrents through barriers, Adv. Phys. **14**, 419 (1965).
[3] M. Tinkham, *Introduction to Superconductivity*, 2nd ed. (Dover Publications, New York, 2004).
[4] J. E. Mooij, T. P. Orlando, L. Levitov, L. Tian, C. H. van der Wal, and S. Lloyd, Josephson persistent-current qubit, Science **285**, 1036 (1999).
[5] J. M. Martinis, S. Nam, J. Aumentado, and C. Urbina, Rabi oscillations in a large Josephson-junction qubit, Phys. Rev. Lett. **89**, 117901 (2002).
[6] J. Koch, T. M. Yu, J. Gambetta, A. A. Houck, D. I. Schuster, J. Majer, A. Blais, M. H. Devoret, S. M. Girvin, and R. J. Schoelkopf, Charge-insensitive qubit design derived from the Cooper pair box, Phys. Rev. A **76**, 042319 (2007).
[7] Y. Makhlin, G. Schön, and A. Shnirman, Quantum-state engineering with Josephson-junction devices, Rev. Mod. Phys. **73**, 357 (2001).
[8] J. Clarke and F. K. Wilhelm, Superconducting quantum bits, Nature (London) **453**, 1031 (2008).
[9] R. C. Jaklevic, J. Lambe, A. H. Silver, and J. E. Mercereau, Quantum interference effects in Josephson tunneling, Phys. Rev. Lett. **12**, 159 (1964).

[10] D. Cohen, Magnetoencephalography: Detection of the brain's electrical activity with a superconducting magnetometer, Science **175**, 664 (1972).

[11] R. L. Fagaly, Superconducting quantum interference device instruments and applications, Rev. Sci. Instrum. **77**, 101101 (2006).

[12] A. Peacock, P. Verhoeve, N. Rando, A. van Dordrecht, B. G. Taylor, C. Erd, M. A. C. Perryman, R. Venn, J. Howlett, D. J. Goldie, J. Lumley, and M. Wallis, Single optical photon detection with a superconducting tunnel junction, Nature (London) **381**, 135 (1996).

[13] Y.-F. Chen, D. Hover, S. Sendelbach, L. Maurer, S. T. Merkel, E. J. Pritchett, F. K. Wilhelm, and R. McDermott, Microwave photon counter based on Josephson junctions, Phys. Rev. Lett. **107**, 217401 (2011).

[14] E. D. Walsh, W. Jung, G.-H. Lee, D. K. Efetov, B.-I. Wu, K.-F. Huang, T. A. Ohki, T. Taniguchi, K. Watanabe, P. Kim, D. Englund, and K. C. Fong, Josephson junction infrared single-photon detector, Science **372**, 409 (2021).

[15] Y.-J. Doh, J. A. Van Dam, A. L. Roest, E. P. A. M. Bakkers, L. P. Kouwenhoven, and S. De Franceschi, Tunable supercurrent through semiconductor nanowires, Science **309**, 272 (2005).

[16] J. A. van Dam, Y. V. Nazarov, E. P. A. M. Bakkers, S. De Franceschi, and L. P. Kouwenhoven, Supercurrent reversal in quantum dots, Nature (London) **442**, 667 (2006).

[17] V. Mourik, K. Zuo, S. M. Frolov, S. R. Plissard, E. P. A. M. Bakkers, and L. P. Kouwenhoven, Signatures of Majorana fermions in hybrid superconductor-semiconductor nanowire devices, Science **336**, 1003 (2012).

[18] W. Chang, S. M. Albrecht, T. S. Jespersen, F. Kuemmeth, P. Krogstrup, J. Nygård, and C. M. Marcus, Hard gap in epitaxial semiconductor–superconductor nanowires, Nat. Nanotechnol. **10**, 232 (2015).

[19] V. V. Ryazanov, V. A. Oboznov, A. Yu. Rusanov, A. V. Veretennikov, A. A. Golubov, and J. Aarts, Coupling of two superconductors through a ferromagnet: Evidence for a π junction, Phys. Rev. Lett. **86**, 2427 (2001).

[20] T. Kontos, M. Aprili, J. Lesueur, F. Genêt, B. Stephanidis, and R. Boursier, Josephson junction through a thin ferromagnetic layer: Negative coupling, Phys. Rev. Lett. **89**, 137007 (2002).

[21] H. Sellier, C. Baraduc, F. Lefloch, and R. Calemczuk, Half-integer Shapiro steps at the 0 - π crossover of a ferromagnetic Josephson junction, Phys. Rev. Lett. **92**, 257005 (2004).

[22] F. S. Bergeret, A. F. Volkov, and K. B. Efetov, Odd triplet superconductivity and related phenomena in superconductor-ferromagnet structures, Rev. Mod. Phys. **77**, 1321 (2005).

[23] A. I. Buzdin, Proximity effects in superconductor-ferromagnet heterostructures, Rev. Mod. Phys. **77**, 935 (2005).

[24] V. A. Oboznov, V. V. Bol'ginov, A. K. Feofanov, V. V. Ryazanov, and A. I. Buzdin, Thickness dependence of the Josephson ground states of superconductor-ferromagnet-superconductor junctions, Phys. Rev. Lett. **96**, 197003 (2006).

[25] A. Buzdin, Direct coupling between magnetism and superconducting current in the Josephson φ_0 junction, Phys. Rev. Lett. **101**, 107005 (2008).

[26] J. W. A. Robinson, J. D. S. Witt, and M. G. Blamire, Controlled injection of spin-triplet supercurrents into a strong ferromagnet, Science **329**, 59 (2010).

[27] T. I. Larkin, V. V. Bol'ginov, V. S. Stolyarov, V. V. Ryazanov, I. V. Vernik, S. K. Tolpygo, and O. A. Mukhanov, Ferromagnetic Josephson switching device with high characteristic voltage, Appl. Phys. Lett. **100**, 222601 (2012).

[28] B. Baek, W. H. Rippard, S. P. Benz, S. E. Russek, and P. D. Dresselhaus, Hybrid superconducting-magnetic memory device using competing order parameters, Nat. Commun. **5**, 3888 (2014).

[29] L. P. Rokhinson, X. Liu, and J. K. Furdyna, The fractional a.c. Josephson effect in a semiconductor–superconductor nanowire as a signature of Majorana particles, Nat. Phys. **8**, 795 (2012).

[30] D. I. Pikulin and Y. V. Nazarov, Phenomenology and dynamics of a Majorana Josephson junction, Phys. Rev. B **86**, 140504(R) (2012).

[31] B. van Heck, A. R. Akhmerov, F. Hassler, M. Burrello, and C. W. J. Beenakker, Coulomb-assisted braiding of Majorana fermions in a Josephson junction array, New J. Phys. **14**, 035019 (2012).

[32] M. Houzet, J. S. Meyer, D. M. Badiane, and L. I. Glazman, Dynamics of Majorana states in a topological Josephson junction, Phys. Rev. Lett. **111**, 046401 (2013).

[33] C. Schrade, A. A. Zyuzin, J. Klinovaja, and D. Loss, Proximity-induced π Josephson junctions in topological insulators and Kramers pairs of Majorana fermions, Phys. Rev. Lett. **115**, 237001 (2015).

[34] K. Flensberg, F. von Oppen, and A. Stern, Engineered platforms for topological superconductivity and Majorana zero modes, Nat. Rev. Mater. **6**, 944 (2021).

[35] T. D. Clark, R. J. Prance, and A. D. C. Grassie, Feasibility of hybrid Josephson field effect transistors, J. Appl. Phys. **51**, 2736 (1980).

[36] H. Takayanagi and T. Kawakami, Superconducting proximity effect in the native inversion layer on InAs, Phys. Rev. Lett. **54**, 2449 (1985).

[37] T. Akazaki, H. Takayanagi, J. Nitta, and T. Enoki, A Josephson field effect transistor using an InAs-inserted-channel $In_{0.52}Al_{0.48}As/In_{0.53}Ga_{0.47}As$ inverted modulation-doped structure, Appl. Phys. Lett. **68**, 418 (1996).

[38] F. Barati, J. P. Thompson, M. C. Dartiailh, K. Sardashti, W. Mayer, J. Yuan, K. Wickramasinghe, K. Watanabe, T. Taniguchi, H. Churchill, and J. Shabani, Tuning supercurrent in Josephson field-effect transistors using h-BN dielectric, Nano Lett. **21**, 1915 (2021).

[39] A. Leblanc, C. Tangchingchai, Z. Sadre Momtaz, E. Kiyooka, J.-M. Hartmann, F. Gustavo, J.-L. Thomassin, B. Brun, V. Schmitt, S. Zihlmann, R. Maurand, É. Dumur, S. De Franceschi, and F. Lefloch, Gate- and flux-tunable $\sin(2\varphi)$ Josephson element with planar-Ge junctions, Nat. Commun. **16**, 1010 (2025).

[40] F. Wen, J. Shabani, and E. Tutuc, Josephson junction field-effect transistors for Boolean logic cryogenic applications, IEEE Trans. Electron Devices **66**, 5367 (2019).

[41] Y. Xiong and K. Delfanazari, Silicon-based Josephson junction field-effect transistors enabling cryogenic logic and quantum technologies, arXiv:2510.25208.

[42] M. Dawber, K. M. Rabe, and J. F. Scott, Physics of thin-film ferroelectric oxides, Rev. Mod. Phys. **77**, 1083 (2005).

[43] N. Setter, D. Damjanovic, L. Eng, G. Fox, S. Gevorgian, S. Hong, A. Kingon, H. Kohlstedt, N. Y. Park, G. B. Stephenson, I. Stolitchnov, A. K. Taganstev, D. V. Taylor, T. Yamada, and S. Streiffer, Ferroelectric thin films: Review of materials, properties, and applications, J. Appl. Phys. **100**, 051606 (2006).

[44] J. F. Scott, Applications of modern ferroelectrics, Science **315**, 954 (2007).
[45] T. S. Böscke, J. Müller, D. Bräuhaus, U. Schröder, and U. Böttger, Ferroelectricity in hafnium oxide thin films, Appl. Phys. Lett. **99**, 102903 (2011).
[46] T. S. Böscke, J. Müller, D. Bräuhaus, U. Schröder, and U. Böttger, Ferroelectricity in hafnium oxide: CMOS compatible ferroelectric field effect transistors, in *2011 International Electron Devices Meeting* (IEEE, Piscataway, NJ, 2011), pp. 24.5.1–24.5.4.
[47] L. W. Martin and A. M. Rappe, Thin-film ferroelectric materials and their applications, Nat. Rev. Mater. **2**, 16087 (2016).
[48] A. I. Khan, A. Keshavarzi, and S. Datta, The future of ferroelectric field-effect transistor technology, Nat. Electron. **3**, 588 (2020).
[49] T. Mikolajick, S. Slesazeck, H. Mulaosmanovic, M. H. Park, S. Fichtner, P. D. Lomenzo, M. Hoffmann, and U. Schroeder, Next generation ferroelectric materials for semiconductor process integration and their applications, J. Appl. Phys. **129**, 100901 (2021).
[50] U. Schroeder, M. H. Park, T. Mikolajick, and C. S. Hwang, The fundamentals and applications of ferroelectric HfO_2, Nat. Rev. Mater. **7**, 653 (2022).
[51] M. Ye. Zhuravlev, R. F. Sabirianov, S. S. Jaswal, and E. Y. Tsymbal, Giant electroresistance in ferroelectric tunnel junctions, Phys. Rev. Lett. **94**, 246802 (2005).
[52] V. Garcia, S. Fusil, K. Bouzehouane, S. Enouz-Vedrenne, N. D. Mathur, A. Barthélémy, and M. Bibes, Giant tunnel electroresistance for non-destructive readout of ferroelectric states, Nature (London) **460**, 81 (2009).
[53] P. Maksymovych, S. Jesse, P. Yu, R. Ramesh, A. P. Baddorf, and S. V. Kalinin, Polarization control of electron tunneling into ferroelectric surfaces, Science **324**, 1421 (2009).
[54] A. Gruverman, D. Wu, H. Lu, Y. Wang, H. W. Jang, C. M. Folkman, M. Ye. Zhuravlev, D. Felker, M. Rzchowski, C.-B. Eom, and E. Y. Tsymbal, Tunneling electroresistance effect in ferroelectric tunnel junctions at the nanoscale, Nano Lett. **9**, 3539 (2009).
[55] V. Garcia and M. Bibes, Ferroelectric tunnel junctions for information storage and processing, Nat. Commun. **5**, 4289 (2014).
[56] H. Ryu, H. Wu, F. Rao, and W. Zhu, Ferroelectric tunneling junctions based on aluminum oxide/ zirconium-doped hafnium oxide for neuromorphic computing, Sci. Rep. **9**, 20383 (2019).
[57] Z. Wang, H. Wu, G. W. Burr, C. S. Hwang, K. L. Wang, Q. Xia, and J. J. Yang, Resistive switching materials for information processing, Nat. Rev. Mater. **5**, 173 (2020).
[58] J. Zhu, T. Zhang, Y. Yang, and R. Huang, A comprehensive review on emerging artificial neuromorphic devices, Appl. Phys. Rev. **7**, 011312 (2020).
[59] T. Mikolajick, M. H. Park, L. Begon-Lours, and S. Slesazeck, From ferroelectric material optimization to neuromorphic devices, Adv. Mater. **35**, 2206042 (2023).
[60] A. Paghi, L. Borgongino, E. Strambini, G. De Simoni, L. Sorba, and F. Giazotto, The ferroelectric superconducting field effect transistor, arXiv:2507.04773.
[61] M. Nadeem, M. S. Fuhrer, and X. Wang, The superconducting diode effect, Nat. Rev. Phys. **5**, 558 (2023).
[62] F. Ando, Y. Miyasaka, T. Li, J. Ishizuka, T. Arakawa, Y. Shiota, T. Moriyama, Y. Yanase, and T. Ono, Observation of superconducting diode effect, Nature (London) **584**, 373 (2020).
[63] H. Wu, Y. Wang, Y. Xu, P. K. Sivakumar, C. Pasco, U. Filippozzi, S. S. P. Parkin, Y.-J. Zeng, T. McQueen, and M. N. Ali, The field-free Josephson diode in a van der Waals heterostructure, Nature (London) **604**, 653 (2022).
[64] C. Baumgartner, L. Fuchs, A. Costa, S. Reinhardt, S. Gronin, G. C. Gardner, T. Lindemann, M. J. Manfra, P. E. Faria Junior, D. Kochan, J. Fabian, N. Paradiso, and C. Strunk, Supercurrent rectification and magnetochiral effects in symmetric Josephson junctions, Nat. Nanotechnol. **17**, 39 (2022).
[65] M. Trahms, L. Melischek, J. F. Steiner, B. Mahendru, I. Tamir, N. Bogdanoff, O. Peters, G. Reecht, C. B. Winkelmann, F. Von Oppen, and K. J. Franke, Diode effect in Josephson junctions with a single magnetic atom, Nature (London) **615**, 628 (2023).
[66] B. Pal, A. Chakraborty, P. K. Sivakumar, M. Davydova, A. K. Gopi, A. K. Pandeya, J. A. Krieger, Y. Zhang, M. Date, S. Ju, N. Yuan, N. B. M. Schröter, L. Fu, and S. S. P. Parkin, Josephson diode effect from Cooper pair momentum in a topological semimetal, Nat. Phys. **18**, 1228 (2022).
[67] M. A. Badarne, E. G. Dalla Torre, and Y. Ivry, Hybrid superconducting-ferroelectric quantum memristor, Phys. Rev. Res. **7**, 043234 (2025).
[68] Y. Tang, N. ten Haaf, A. Bondarenko, M. N. Ali, and Y. M. Blanter, Pseudo-diode effect in a ferroelectric Josephson junction (unpublished).
[69] R. R. Mehta, B. D. Silverman, and J. T. Jacobs, Depolarization fields in thin ferroelectric films, J. Appl. Phys. **44**, 3379 (1973).
[70] J. E. Hirsch, Charge expulsion and electric field in superconductors, Phys. Rev. B **68**, 184502 (2003).
[71] J. E. Hirsch, Electrodynamics of superconductors, Phys. Rev. B **69**, 214515 (2004).
[72] J. Hirsch, Reply to "comment on 'charge expulsion and electric field in superconductors"', Phys. Rev. B **70**, 226504 (2004).
[73] G. De Simoni, F. Paolucci, P. Solinas, E. Strambini, and F. Giazotto, Metallic supercurrent field-effect transistor, Nat. Nanotechnol. **13**, 802 (2018).
[74] V. Ambegaokar and A. Baratoff, Tunneling between superconductors, Phys. Rev. Lett. **10**, 486 (1963).
[75] J. G. Simmons, Generalized formula for the electric tunnel effect between similar electrodes separated by a thin insulating film, J. Appl. Phys. **34**, 1793 (1963).
[76] P. L. Richards and M. Tinkham, Far-infrared energy gap measurements in bulk superconducting In, Sn, Hg, Ta, V, Pb, and Nb, Phys. Rev. **119**, 575 (1960).
[77] R. Prozorov, M. Zarea, and J. A. Sauls, Niobium in the clean limit: An intrinsic type-I superconductor, Phys. Rev. B **106**, L180505 (2022).
[78] C. Kittel and P. McEuen, *Introduction to Solid State Physics* (John Wiley & Sons, 2018).
[79] J. Rodríguez Contreras, H. Kohlstedt, U. Poppe, R. Waser, C. Buchal, and N. A. Pertsev, Resistive switching in metal–ferroelectric–metal junctions, Appl. Phys. Lett. **83**, 4595 (2003).
[80] M. Ye. Zhuravlev, Y. Wang, S. Maekawa, and E. Y. Tsymbal, Tunneling electroresistance in ferroelectric tunnel junctions with a composite barrier, Appl. Phys. Lett. **95**, 052902 (2009).

[81] A. Belianinov, Q. He, A. Dziaugys, P. Maksymovych, E. Eliseev, A. Borisevich, A. Morozovska, J. Banys, Y. Vysochanskii, and S. V. Kalinin, $CuInP_2S_6$ room temperature layered ferroelectric, Nano Lett. **15**, 3808 (2015).

[82] S. Zhou, L. You, A. Chaturvedi, S. A. Morris, J. S. Herrin, N. Zhang, A. Abdelsamie, Y. Hu, J. Chen, and Y. Zhou, Anomalous polarization switching and permanent retention in a ferroelectric ionic conductor, Mater. Horiz. **7**, 263 (2020).

[83] S. Zhou, L. You, H. Zhou, Y. Pu, Z. Gui, and J. Wang, Van der Waals layered ferroelectric $CuInP_2S_6$: Physical properties and device applications, Front. Phys. **16**, 13301 (2021).

[84] M. H. Park, Y. H. Lee, H. J. Kim, Y. J. Kim, T. Moon, K. D. Kim, J. Müller, A. Kersch, U. Schroeder, T. Mikolajick, and C. S. Hwang, Ferroelectricity and antiferroelectricity of doped thin HfO_2-based films, Adv. Mater. **27**, 1811 (2015).

[85] M. H. Park, C.-C. Chung, T. Schenk, C. Richter, M. Hoffmann, S. Wirth, J. L. Jones, T. Mikolajick, and U. Schroeder, Origin of temperature-dependent ferroelectricity in Si-doped HfO_2, Adv. Electron. Mater. **4**, 1700489 (2018).

[86] Y. Tang, M. Ali, G. Bauer, and Y. Blanter, Polarization controlled supercurrent in ferroelectric Josephson junction, Zenodo (2025), doi: 10.5281/zenodo.17650000.